IOP Publishing Journal of Physics D: Applied Physics
J. Phys. D: Appl. Phys. **55** (2022) 375202 (10pp) https://doi.org/10.1088/1361-6463/ac7bb8

Experimental study on the effect of argon shielding gas on the suppression of nitrogen arc anode ablation

Ya-Hao Hu[1,2], Xian Meng[2,*], He-Ji Huang[2], Ke Shao[1,2], Anthony B Murphy[3], Kai Huang[1], Su-Rong Sun[1] and Hai-Xing Wang[1,*]

[1] School of Astronautics, Beihang University, Beijing 100191, People's Republic of China
[2] Institute of Mechanics, Chinese Academy of Sciences, Beijing 100190, People's Republic of China
[3] CSIRO Manufacturing, PO Box 218, Lindfield, NSW 2070, Australia

E-mail: menxian@imech.ac.cn and whx@buaa.edu.cn

Received 13 April 2022, revised 11 June 2022
Accepted for publication 23 June 2022
Published 5 July 2022

Abstract

The high heat flux density of the DC arc often leads to severe anode ablation, which is a key factor limiting the wider use of the DC plasma torches. In this study, a series of comparative experimental studies are conducted with the goal of suppressing nitrogen arc anode ablation by combining argon shielding flow and anode structure. It is found that for the planar electrode structure, the use of argon shielding gas can alleviate the ablation of the anode by nitrogen arc to some extent. If a boron nitride channel is installed on the anode surface to constrain the argon shielding flow, the electrode ablation can be significantly reduced. The experimental results show that there is no significant ablation on the anode surface after 1 h of operation of the nitrogen arc device with an arc current of 100 A. Further analysis reveals that, on the one hand, argon shielding gas can extend the range of motion of the nitrogen arc root along the anode surface and increase the speed of arc root motion, which has the effect of expanding the time-averaged arc anode attachment area. On the other hand, argon shielding gas can also increase the size of the nitrogen arc root and decrease the temperature of the arc root. The use of constraining channels can effectively control the range of motion of the arc root along the anode surface and strengthen the influence of argon shielding gas. The combination of these effects can substantially suppress the anode ablation of the DC arc device.

Keywords: nitrogen arc, anode ablation, arc anode attachment, DC arc

(Some figures may appear in colour only in the online journal)

1. Introduction

As a high-temperature heat source commonly used in industrial applications such as materials processing, aerospace propulsion and waste processing, arc plasmas typically have core temperatures higher than 10 000 K [1–4]. During the operation of an arc plasma torch, the peak current density of the arc may be as high as 10^8 A m^{-2} and the peak heat flow density as high as 10^8 W m^{-2} in the arc attachment region on the anode [5–7]. Such a high heat flux density often leads to severe anode ablation and poor arc stability. Therefore, the anode ablation caused by the arc is a critical issue in many applications of plasma torches, often determining the reliability and service life of the arc equipment.

Previous numerous experimental studies and numerical simulations have shown that the arc may attach to the anode in a diffuse or constricted mode [8–11]. If the arc-forming gas is a molecular gas, such as the widely used nitrogen, the arc is usually attached to the anode in a constricted mode. The area of the arc attachment zone is usually much smaller than that in the case of diffuse arc attachment, resulting in particularly

* Authors to whom any correspondence should be addressed.

severe anode ablation. Therefore, many techniques have been developed to reduce the anode ablation and improve the stability of the arc plasma. These techniques include rotating the arc using an external magnetic field [12–14], the use of a multi-electrode structure [15, 16], and the gas-dynamic dispersion method [17, 18].

The magnetically rotated arc can be used to produce a large area of homogeneous discharge, called the magnetically dispersed arc. At the same time, the arc root also rotates at high speed under the action of the external magnetic field [13, 19, 20]. The method leads to a limited expansion of the time-averaged arc anode attachment area.

The plasma torch with the multiple-anode structure operates with fixed anode roots. The input power for each of the separated arc roots is reduced since the anode current is divided among the anodes, reducing the current density and heat flux density in each arc attachment region [15, 16].

The gas-dynamic dispersed arc plasma torch combines the anode structure with a constricting and expansion (also known as a converging-diverging) nozzle, with the gas-dynamic force expanding and dispersing the arc. The experimental results show that even for pure nitrogen arcs, diffuse arc attachment can be achieved on the surface of a water-cooled anode. This indicates that the method can also effectively reduce the anode thermal heat load and improve the anode life and arc stability [17, 18, 21].

All of the above methods have been successfully applied and have significantly increased our knowledge and understanding of the method to mitigate anode ablation. Nevertheless, they all require more complex torch designs. From the standpoint of practical applications, a more stable and long-lived DC arc plasma torch that does not have a more complex structure and system is desirable.

In many applications, nitrogen is used as the arc-forming gas to increase the torch power and the enthalpy of the arc plasma jet. Previous studies have also shown that if argon is used as the shielding gas, the stability of the arc is improved, and anode ablation can be reduced to some extent [22, 23]. However, the mechanisms by which the combination of the shielding gas and nitrogen arc reduces the anode ablation are not fully understood, and further study is needed to investigate the effect of argon on the nitrogen arc attachment behaviour.

Based on the above discussion, the main objective of this study is to investigate how to tailor the argon gas flow to play an effective role in suppressing the nitrogen arc ablation at the anode. To facilitate direct observation, a transferred arc device is used in the experiments. A high-speed camera and spectroscopic measurements are used to study the attachment behaviour of the arc under different conditions and its effect on the anode ablation. The results of this study can provide a basis for further improving the design of the DC arc plasma torch.

2. Experimental setup

The general layout of the experimental system used in this study is shown in figure 1. The whole system includes three main components. First, the arc chamber system is used to contain the arc-forming gas and maintain atmospheric pressure. The second component is the power and gas supply systems. Third, the high-speed camera and the spectral measurement system are used to photograph the arc's dynamic behaviour and obtain the arc temperature distribution.

As shown in figure 1, the transferred arc device is placed in an experimental chamber with a diameter of 600 mm and a height of 550 mm. The thoriated tungsten cathode is a 5 mm diameter cylinder with a 60° cone angle at its tip portion. Two copper anodes with different structures are used. One is a planar anode, and the other is an anode with a boron nitride (BN) constraining channel for confining the argon shielding gas. The main reason for choosing BN as constraining channel's material is that it is an insulator and can withstand high temperatures. And the two opposite side walls of the BN limit the lateral divergence of the argon shielding gas on the anode, which is helpful to improve the protective effect of the argon shielding gas. The two anode structures used in this experiment and the dimensions of the constraining channel are shown in figure 2. In the experiment, the water-cooled cathode and the water-cooled copper anode are placed parallel to each other with a separation of 5 mm, chosen to simulate the relative position of the two electrodes inside the DC arc plasma torch. The cooling water temperature is maintained within the range of 20 °C–24 °C during the experiment.

An IGBT inverter DC constant-current power supply with a rated power of 20 kW and an unload voltage of 450 V is used, and the current is adjustable in the range of 40–160 A. In the experiments reported here, the operating arc current was fixed at 100 A, the arc-forming gas was nitrogen, and argon was used as the shielding gas. The arc-forming gas was supplied through the channel between the cathode and the alumina ceramic nozzle. The shielding gas is provided by a gas distributor, which is placed directly above the anode and below the cathode, as shown in figure 1. The gas distributor has five evenly distributed small holes of 1 mm diameter so that the gas flow direction is parallel to the anode surface. When a planar electrode is used in the experiment, the shielding gas flow along the anode surface is not constrained. For the case with a BN constraining channel, the argon gas enters the channel directly from the gas distributor and the shielding gas flow is constrained by the channel. Before the arc is ignited, the air in the chamber is pumped out by the vacuum pump and the working gas is refilled to 1.0 atm. After igniting the arc, nitrogen as well as argon shielding gas is continuously supplied and the exhaust gas is naturally discharged from the bypass through a check valve. During the experiment, the pressure in the chamber is maintained at around 1.0 atm.

A high-speed camera is used to directly observe the arc behaviour, combined with the emission spectroscopy method to measure the arc temperature. A monochromatic high-speed camera, i-SPEED 513, with a maximum frame rate of 6382 fps at 1920 × 1080 pixels and a minimum exposure time of 1 μs, is used. The frame rate is set to 50 000 fps at 504 × 282 pixels, which is high enough to capture the dynamic behaviour of the arc during the restrike process. Similar to

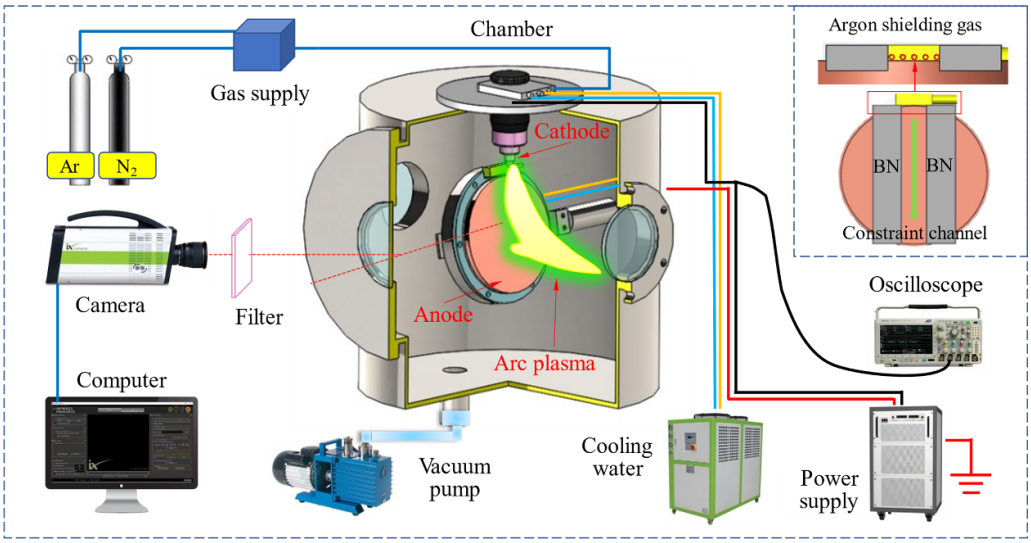

Figure 1. Schematic of the experimental setup.

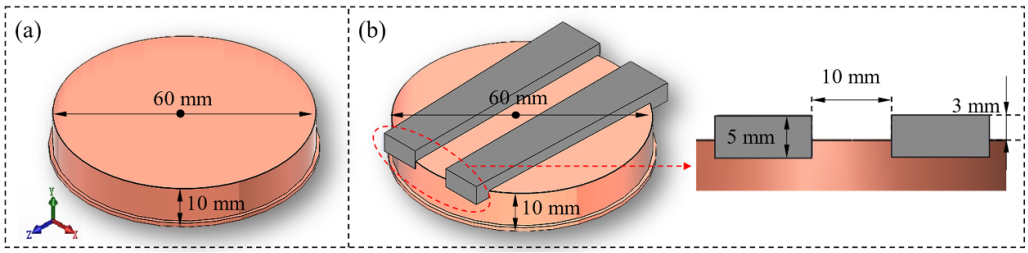

Figure 2. The structure of the anode used in the experiment, (a) planar anode, (b) anode with BN constraining channel.

our previous studies [24, 25], a four-channel spectrometer (AvaSpec-ULS4096CL) with an optical fibre (200 μm) fixed on a displacement stage (accuracy 0.001 mm) is used to record the radial distribution of the emission intensity. The temperature of the argon and nitrogen arcs are measured separately using different wavelengths of the emission spectrum. Two narrow-band filters of 675 nm and 696 nm with a bandwidth of 10 nm are used for the argon plasma. For the nitrogen plasma, 650 nm and 745 nm narrow-band filters with a bandwidth of 10 nm are used. The *in-situ* arc temperature distribution measurement during the arc motion is based on the relative intensity method, which is described in [26–28]. Specific details of the calibration and measurement methods can be found in [24, 25]. The arc voltage is obtained by measuring the voltage difference between the electrodes using a voltage probe (Tektronix TPP0500B) and a digital oscilloscope (Tektronix MDO3034).

3. Results and discussions

3.1. Ablation characteristics of anodes with different structures

A comparative experiment based on a planar anode was conducted to investigate the effect of the presence or absence of argon shielding gas on the ablation characteristics of the anode. As shown in figure 3(a), pure nitrogen was supplied as the arc-forming gas from the annulus between the cathode and the ceramic tube with a flow rate of 10 slm. Argon was supplied as the shielding gas from a gas distributor located below the cathode and immediately above the anode surface. Figure 3(b) shows a photograph of the anode after 5 min of arc operation without argon shielding gas. Figure 3(c) is a photograph of the anode after 5 min of arc operation with 5 slm argon shielding gas. Before the experiment, The anode surface is processed by turning, and the anode surface roughness is Ra6.3 (which means the countour arithmetic mean deviation of the machined surface is 6.3 μm). From figures 3(b) and (c), we can observe the trajectory of the arc root on the anode surface and the ablation degree. Based on the analysis of the trajectory of the arc root in both cases, it can be seen that the arc runs in the restrike mode. As the arc root moves downstream, the movement range of the arc root also gradually extends and spreads. For the transferred arc used in this study, in which the cathode is parallel to the anode, the arc is attached perpendicular to the anode surface and is subjected to a pulling down drag force exerted by the cold flow in the boundary layer and the Lorentz force due to the self-magnetic field induced by the curvature of the current flow. The Lorentz force may act in the same or opposite direction as the flow drag force depending on the curvature of the current in the anode arc root. Under

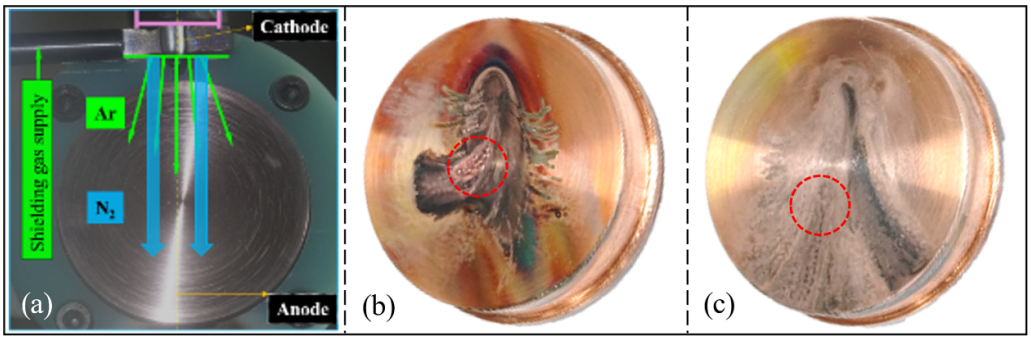

Figure 3. Effect of the presence or absence of the argon shielding gas on electrode ablation in the case of a planar electrode, (a) configuration of electrode and shielding gas distributor, (b) anode condition after the experiment without shielding gas, (c) anode condition after the experiment with shielding gas.

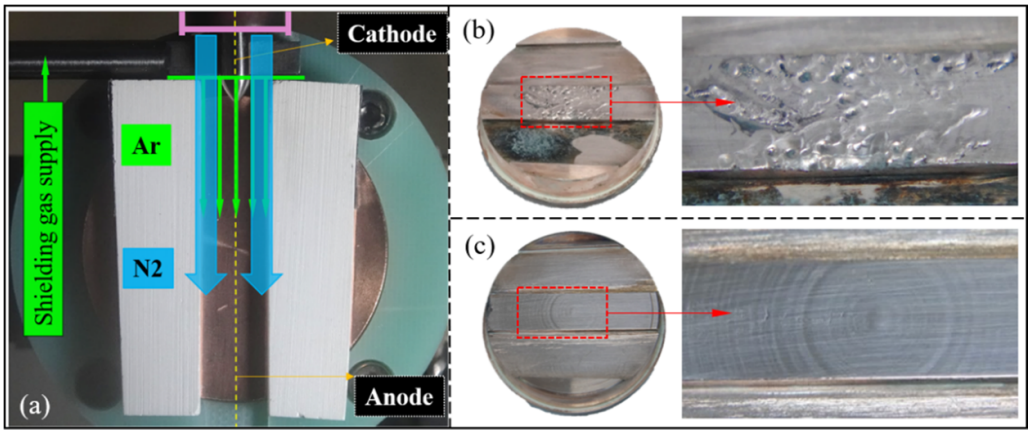

Figure 4. Effect of the presence or absence of the argon shielding gas on electrode ablation in the case of the anode with BN constraining channel, (a) configuration of electrode and shielding gas distributor, (b) anode condition after the experiment without shielding gas, (c) anode condition after the experiment with shielding gas.

the combined action of these forces, the anode arc attachment will generally exhibit an axial and rotational movement on the anode surface. The axial movement of the arc root is the main reason for the formation of the arc restrike attachment mode, while the rotation of the arc usually leads to the lateral movement of the arc root, as shown in figures 3(b) and (c).

For the case of without argon shielding gas, significant melt locations can be observed on the anode surface, and the depth of the ablation crater is about 0.5 mm. For the case of with argon shielding gas, the ablation range of the anode is expanded, but the ablation degree is reduced, the ablation crater depth is also reduced to about 0.1 mm. Comparing the degree of ablation in the two cases, it can be seen that the presence of argon shielding gas can indeed alleviate the anode ablation to a certain extent. However, the shielding-gas arrangement does not avoid anode ablation.

From the above experiments, it can be observed that although using argon shielding gas can alleviate the ablation of the planar anode, the large arrange of motion of the arc root decreases the effectiveness of argon shielding gas in protecting the anode. Therefore, a constraining channel is introduced along the direction of the arc root movement to constrain the argon shielding gas and the arc motion to assess whether this can suppress the anode ablation significantly. Figure 4(a) shows the configuration of the anode with a BN channel and the configuration of the gas supply. The depth of the BN channel is 3 mm, and the width is 10 mm. In the following experiments, pure nitrogen was still used as the arc-forming gas with a flow rate of 10 slm and the argon shielding gas flow rate was set to 5 slm. Figure 4(b) shows a photograph of the anode after 5 min of arc operation without argon shielding gas. Figure 4(c) presents a photograph of the anode after 1 h of arc operation with 5 slm argon shielding gas. It should be pointed out that the 1 h run in figure 4(c) is the cumulative time, not completed at once. Because of the high power of the nitrogen arc operation, the entire arc chamber is heated up significantly in a short time, so the experiment is divided into four runs of 15 min each, waiting for the chamber to cool down before starting the next run. We also tried to enhance the cooling of the chamber and continued the experiment for 20 min. The anode also showed almost no ablation after the experiment. Therefore, the experiments can last much longer if the chamber could be sufficiently cooled.

As can be seen in figure 4(b), the range of motion of the arc root is significantly limited by the BN constraining channel. In the absence of shielding gas protection, the anode ablation is more severe than without the channel. However, if argon shielding gas is present, then even after 1 h operation of the

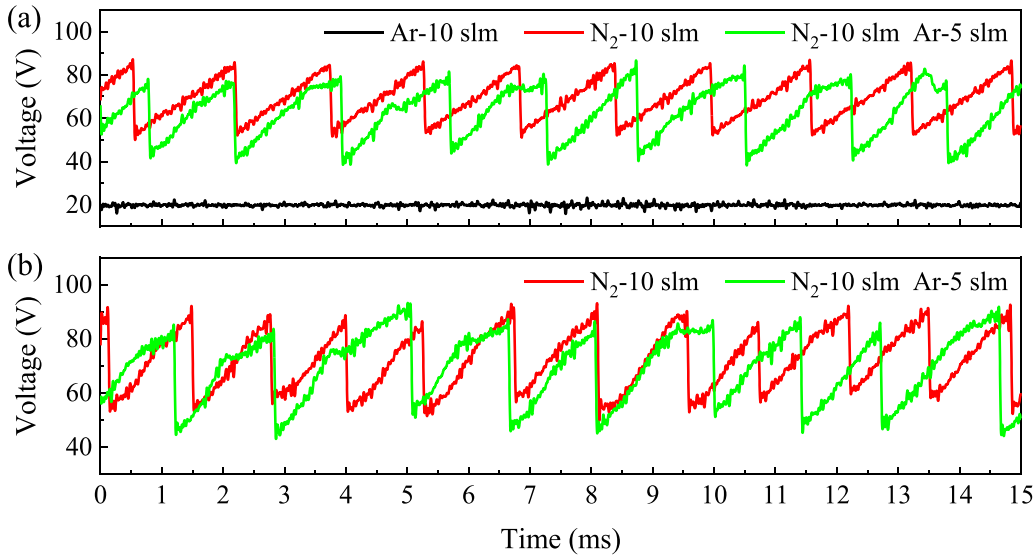

Figure 5. Arc voltage waveforms for (a) planar anode, (b) anode with BN constraining channel.

arc device, there are still no obvious signs of ablation on the anode surface, as can be seen in figure 4(c), indicating that the combination of shielding gas and constraining channel works well to suppress the anode ablation. It should be noted that the increased gasdynamic force due to the confining effect of the BN constraining channel leads to an increase in the axial range of motion of the arc root and a higher arc voltage than the planar electrode case for the BN constraining channel condition. Since the current is constant, the increase in arc voltage reflects the increase in input power, which may lead to more severe ablation of the anode. On the other hand, even with the increased input power, the confining effect of the BN constraining channel on the argon shielding gas makes it work better to suppress the anode ablation.

In this study, we also conducted the test using nitrogen as the shielding gas of nitrogen arc. The condition of the anode surface after the experiment is similar to figure 4(b). There is severe ablation on the anode, which indicates that the use of nitrogen as shielding gas cannot suppress the ablation of anode.

3.2. Effect of shielding gas on arc root motion characteristics

Figure 5 presents the voltage waveforms recorded for the arc restrike process. To facilitate the comparison of arc characteristics, the voltage evolution curve with pure argon as the arc-forming gas, with a flow rate of 10 slm, is also shown in figure 5. As can be seen from the figure, for the planar anode, when pure argon is used as the arc-forming gas, the arc operation is in steady-state mode, while in the other cases, the nitrogen arcs are in restrike mode and the voltage variation with time shows a typical sawtooth shape.

A comparison of the arc voltage drop and restrike frequencies with and without argon shielding gas is given in figure 6. The 'voltage drop' is the difference between the maxima arc voltage (obtained by averaging the maxima arc voltages collected by the oscilloscope) and the minima arc voltage (obtained by the same way as the maxima arc voltage). The restrike period is obtained by averaging the total time of several consecutive restrike cycles, and the restrike frequency is the reciprocal of the period. In the planar anode case (figure 6(a)), using argon shielding gas in the nitrogen arc causes an increase in the voltage drop during the arc restrike process and a slight decrease in the restrike frequency for the planar anode. From figure 6(b), it can be seen that for the case with a BN constraining channel installed on the anode surface, the voltage drop of the nitrogen arc increases slightly and the restrike frequency decreases more significantly compared to the case without argon shielding gas.

From the above results, it can be seen that the use of argon shielding gas slightly reduces the maximum and minimum arc voltage of the nitrogen arc. Since the arc current remains constant during the experiment, the input power also decreases slightly. The argon shielding gas combined with the constraining channel somewhat reduces the restrike frequency of the nitrogen arc in the channel. However, note that the restrike frequency for the anode with the channel is very close to the restrike frequency in the presence of argon shielding gas at the planar anode. In other words, the presence of the channel does not reduce the restrike frequency of the nitrogen arc.

Photographs of the arc behaviour during nitrogen arc restrike in the case of a planar electrode are given in figure 7. The time 0.0 ms corresponds to the moment when the restrike just occurs. It also corresponds to the rapid drop in arc voltage of the voltage waveform. These pictures are taken under the same shooting conditions with 50 000 fps frame rate, 1 μs exposure time, and F/4.0 aperture. The transmittance of the neutral density filter is 1/64 (ND 1.8). It is important to note that although these photos are overexposed, the arc edges are clearly outlined, which facilitates further analysis and comparison.

Figures 7(A)–(C) presents the dynamic behaviour of the nitrogen arc at different moments of the restrike process: 0.0 ms, 0.2 ms, and 0.5 ms, respectively. Figure 7(A) also

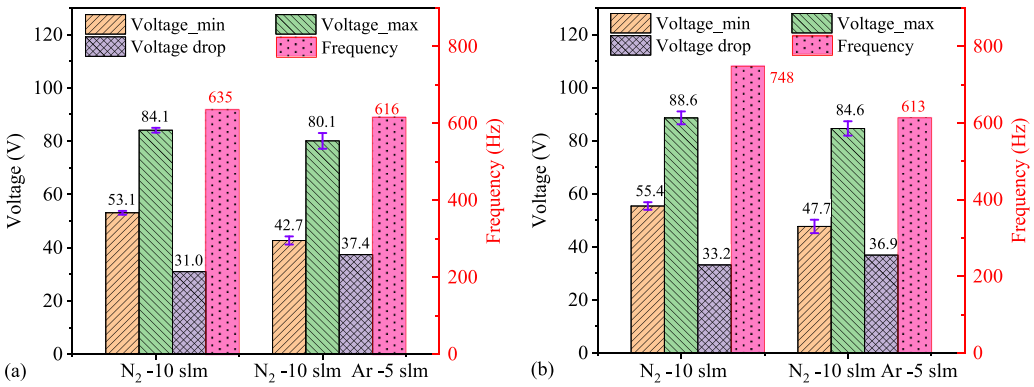

Figure 6. Effect of argon shielding gas on restrike characteristics for (a) planar anode, (b) anode with BN constraining channel.

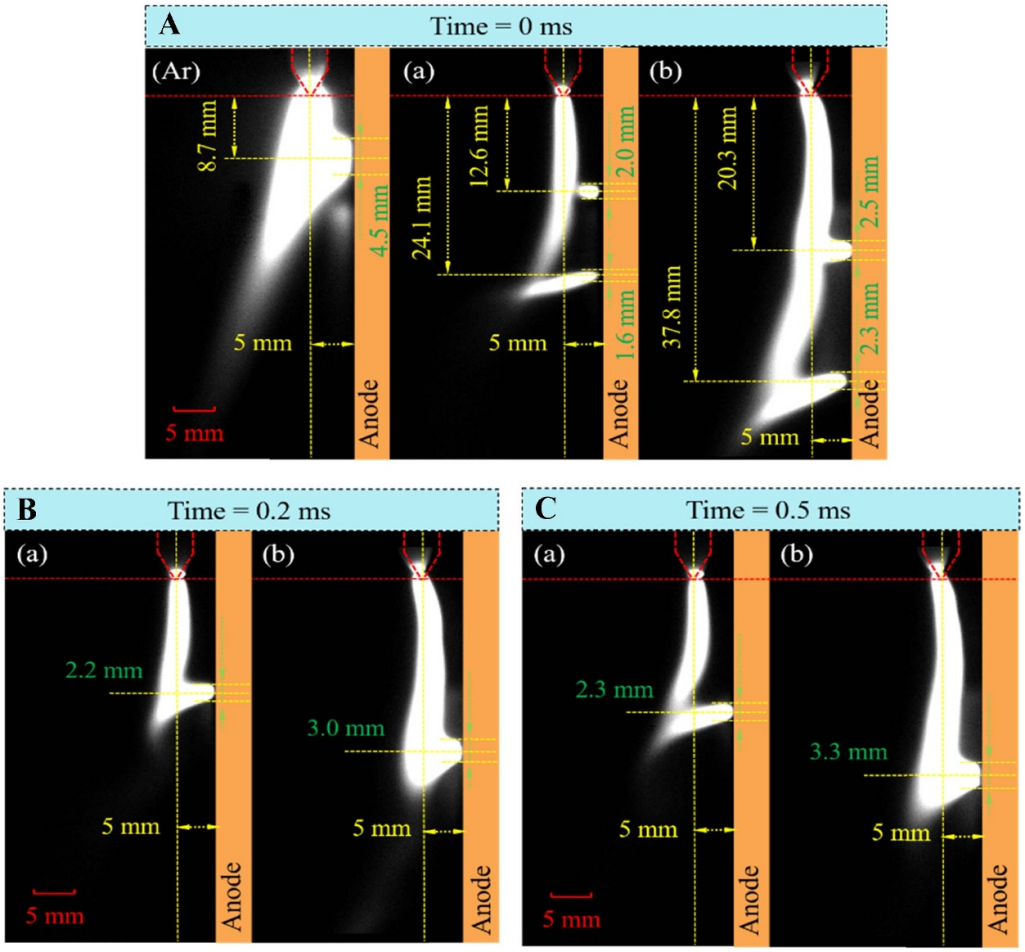

Figure 7. Arc photos for planar anode at different moments, (Ar) pure argon arc with flow rate of 10 slm, (a) pure nitrogen arc with flow rate of 10 slm, (b) nitrogen arc with flow rate of 10 slm and argon shielding gas with flow rate of 5 slm.

includes a photo of the argon arc attachment on the anode, from which it can be seen that the attachment mode of the argon arc differs substantially from that of the nitrogen arc. For a planar anode, the presence or absence of argon shielding gas greatly influences the attachment position of the nitrogen arc at the anode. The introduction of argon shielding gas shifts both the upstream and downstream restrike positions of the nitrogen arc downward, while the distance between the upstream and downstream arc roots also increases. It is also noted that while the argon shielding gas can change the attachment characteristics of the nitrogen arc at the anode, it does not affect the main characteristics of the nitrogen arc column region.

Figure 8 presents photographs of the behaviour of the nitrogen arc at different moments for the anode with the BN constraining channel, with and without argon shielding gas. Due to the finite depth of the channel, the arc luminescence is blocked when viewed from the side. It is not possible to photograph the arc movement and anode attachment state from the

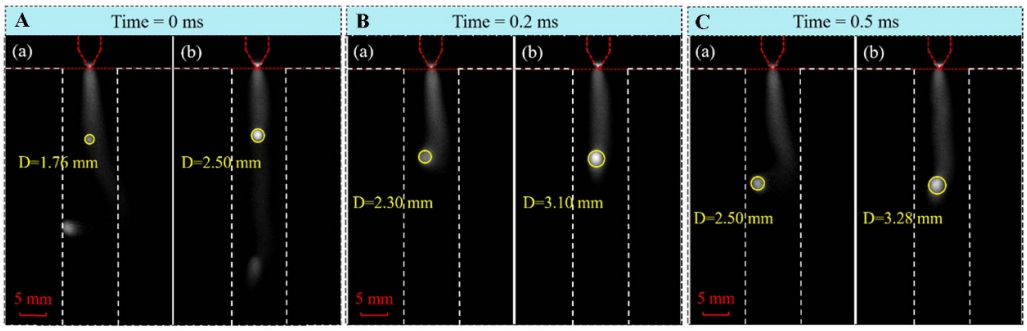

Figure 8. Arc photos for the anode with BN constraining channel at different moments, (a) nitrogen arc with flow rate of 10 slm, (b) nitrogen arc with flow rate 10 slm and argon shielding gas flow of 5 slm.

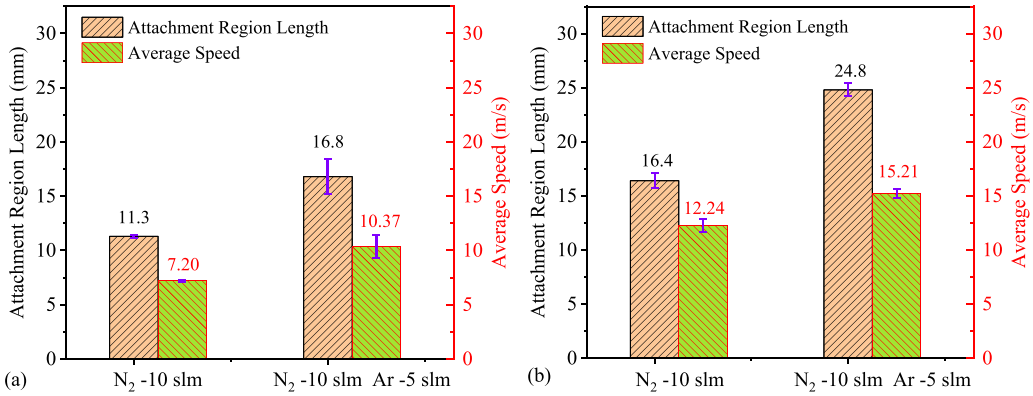

Figure 9. The length of the arc root attachment zone and the average speed of the arc root movement during nitrogen arc restrike, (a) planar anode, (b) anode with BN constraining channel.

side, as was done in figure 7. Therefore, the arc image is taken perpendicular to the anode surface. Since the camera shoots the arc root through the arc, the aperture is reduced to F/16 to avoid the strong light from the arc column obscuring the image of the arc root. In this way, the locations of the arc root at different moments can be obtained. As shown in figure 8(A), the arc roots are located upstream and downstream of the nitrogen arc at the initial moment of restrike. Figures 8(B) and (C) show that only one arc root can be observed 0.2 ms and 0.5 ms after the restrike.

It can be seen from figure 8 that the installation of the BN constraining channel on the anode surface effectively limits the flow of argon shielding gas as well as the extension and divergence of the arc root during its movement. Comparison of figures 8(a) and (b) shows that the introduction of shielding gas has little effect on the upstream arc root position but has a greater effect on the downstream arc root position; that is, the introduction of shielding gas increases the range of motion of the arc root during the restrike process.

The position of the arc root at each moment can be obtained from the high-speed camera images of the arc restrike process, and this can be used to calculate the range of motion of the arc root. The speed of motion of the arc root can be obtained from this data and the period of the arc restrike process, the results are shown in figure 9. From figure 9(a), it can be seen that for the planar anode, the introduction of argon shielding gas significantly increases the range of motion and speed of the nitrogen arc root. As can be seen from figure 9(b), for the case with BN constraining channel, the introduction of argon shielding gas can further increase the range of motion and speed of the nitrogen arc root relative to the planar electrode case.

Based on the above analysis, the introduction of argon shielding gas and the BN constraining channel increase the range of motion of the arc root and the speed of motion, which has the effect of increasing the area over which the arc attaches to the anode.

3.3. Effect of shielding gas on size and temperature of the arc root

In addition to the motion of the arc root, the introduction of argon shielding gas may affect the basic characteristics of the arc root, such as its size and temperature. From the arc movement pictures in figures 7 and 8, one can also obtain further information on the effect of argon shielding gas on the size of the arc root. As shown in figure 7, for the planar anode, the high-speed camera can take pictures from the side of the device to obtain images of the arc movement during the restrike process. To be able to observe the arc root state more clearly, the obtained image is overexposed, and the majority of the arc area has a grey value of 255. The grey gradient at the edge of the arc is large, and the grey value drops from 255 to below 100 within 2–3 pixels. Based on this, we define the boundary of the arc as a grayscale value of 200. The size of the anode arc

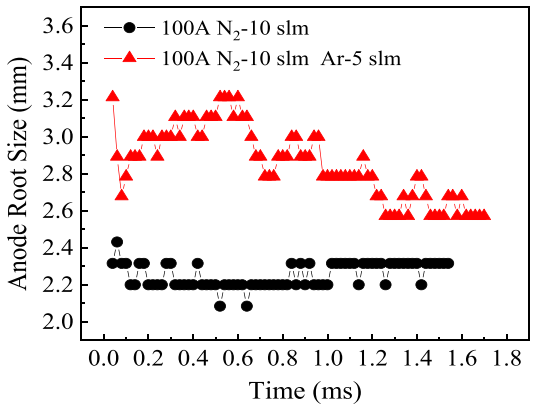

Figure 10. The size of anode arc root in a typical restrike period for the planar anode.

Table 1. Anode arc root size for anode structure with constraining channel.

	Anode arc root size (mm)	
Time (ms)	100 A N_2–10 slm	100 A N_2–10 slm Ar–5 slm
0.0	1.76	2.50
0.2	2.30	3.09
0.5	2.50	3.28
0.8	2.50	3.53
1.2	2.60	3.43

root at the position 1 mm above the anode surface in figure 7 can then be obtained; the results are shown in figure 10.

It is worth noting that there are errors associated with using this method to obtain the arc root size. First, because the shape of the arc root may be irregular, the results taken from one side of the arc may not represent the true size of the arc root; second, the size of the arc root may vary slightly within each arc restrike cycle. However, the method is reasonable for the purpose of comparing the relative size of the arc root with or without shielding gas since the errors are expected to be similar for both cases. The presence or absence of argon shielding gas significantly affects the nitrogen arc root size in the planar electrode case, as shown in figure 10. In a typical restrike period, the arc root size changes less without argon shielding gas. For the case with argon shielding gas, the arc root size of nitrogen arc changes significantly and is always larger than the nitrogen arc root size without shielding gas.

Based on a similar approach, we can extract the size of the arc root from the arc motion images with the constraining channel in figure 8. It is worth noting that the photos are taken perpendicular to the anode surface, so the size of the arc root can be obtained directly. In this case, the selection of the arc root boundary is based on 20% of the maximum grey value at the centre of the anode arc root. Table 1 compares the arc root size in a typical restrike period. The arc root size with argon shielding gas is larger than that without argon shielding gas. This again indicates that adding argon shielding gas to the nitrogen arc can increase the arc root size.

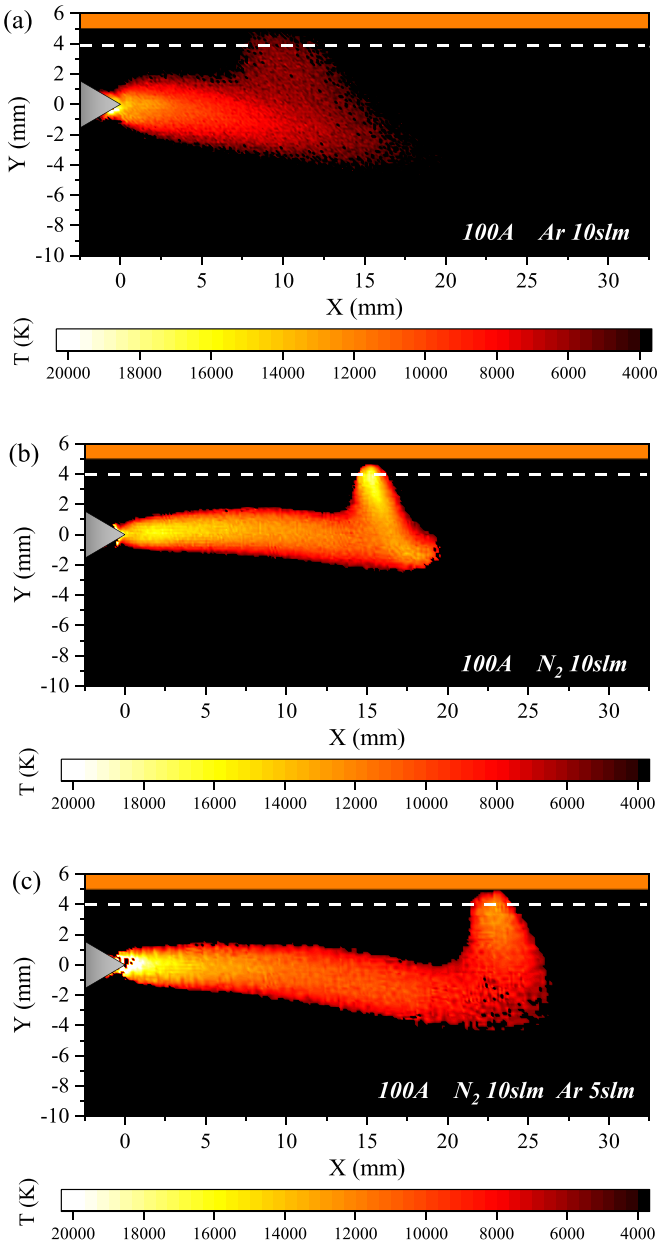

Figure 11. Temperature distribution of (a) pure argon arc, (b) pure nitrogen arc, and (c) nitrogen arc with argon shielding gas in the case of planar electrode.

The argon shielding gas not only changes the size of the arc root, but at the same time, the ionized argon component at the arc root participates in the arc attachment process and affects the temperature of the arc root. Figure 11 shows the temperature distribution of the pure argon arc, pure nitrogen arc, and nitrogen arc with argon shielding gas in the case of the planar electrode. In figure 11(a), the argon arc is in stable attachment mode with an arc voltage of about 19.9 V. The arc in figure 11(b) is nitrogen arc without argon shielding gas 0.2 ms after restrike, and the corresponding arc voltage is about 57.8 V. The arc in figure 11(c) is nitrogen arc with argon shielding gas 0.5 ms after restrike, and the corresponding arc voltage is about 56.4 V. For a clearer comparison, the

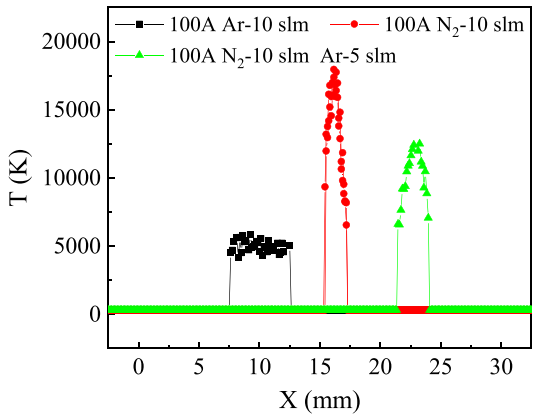

Figure 12. Comparison of the arc root temperature distribution for different cases at a position 1 mm above the planar anode.

temperature distributions of the arc root 1 mm above the planar anode are plotted in figure 12.

Figures 11 and 12 together show that the arc root temperature is lowest when pure argon is the arc-forming gas. For pure nitrogen, the arc root temperature is highest, with the peak temperature reaching more than 17 500 K. The use of argon the shielding gas can significantly reduce the nitrogen arc root temperature, so that the peak arc root temperature is reduced to about 12 500 K, which reduces the conductive heat transfer from the arc to the anode. The arc root temperature cannot be obtained in a similar way due to the blocking of the arc root luminescence by the constraining channel, but we can infer by analogy that argon shielding gas will have the effect of reducing the arc root temperature of the nitrogen arc even for the case with the channel.

In general, using argon shielding gas can change the size, temperature and range of motion of the nitrogen arc root. The two main heat transfer mechanisms to the anode are electron condensation, which is proportional to the current density, and thermal conduction, which depends on the temperature of the arc root. Since the arc root size and temperature are reduced by the flow of argon shielding gas, the heat flux within the attachment region will be decreased. Moreover, the range of motion is larger, so the heat flux is spread over a wider region during a restrike period.

However, if the range of motion of the arc root and the flow of argon shielding gas cannot be controlled, the ablation of the anode cannot be effectively suppressed. The use of the BN constraining channel can effectively suppress the divergence and extension of the arc root and give full play to the shielding effect of argon gas. After the arc device runs for 1 h, there is no obvious ablation of the anode, which proves the effectiveness of the method.

4. Conclusions

This experimental study has explored the use of argon shielding gas in suppressing the anode ablation of nitrogen arcs. The effect of the argon shielding gas on the attachment behaviour and ablation characteristics of the arc was compared for a planar anode and an anode with a BN constraining channel. It was found that the nitrogen arc is always in the restrike mode for the range of experimental parameters explored. For the planar anode, the introduction of the argon shielding gas increased the range of motion of the arc root, increased the size and decreased the temperature of the arc root. However, only using the argon shielding gas still did not effectively suppress electrode ablation because the area of arc motion expands and diverges during the downstream motion of the arc root under aerodynamic action. After the introduction of the BN constraining channel on the anode, the shielding gas has a more obvious effect on the attachment characteristics of the nitrogen arc, increasing the range of motion and speed of the nitrogen arc root, expanding the time-averaged area of attachment of the arc root, and also increasing the size of the arc root. The introduction of the constraining channel effectively limits the range of motion of the arc root and enhances the protective effect of the argon shielding gas on the anode. After 1 h of cumulative operation of the arc device, the anode surface was not significantly ablated, which demonstrates the effectiveness of this method.

The results obtained here, combined with further investigations of the role and effect of the argon shielding gas, will assist the design of a stable and long-life arc plasma torch. The torch will include shielding gas flow and controlled arc attachment characteristics, ideally without a substantial increase in complexity.

Data availability statement

All data that support the findings of this study are included within the article (and any supplementary files).

Acknowledgments

This work was supported by the National Natural Science Foundation of China (Grant Nos. 11735004, 12175011 and 12005010) and Open Funding from State Key Laboratory of High-temperature Gas Dynamics, Chinese Academy of Sciences (No. 2021KF08)

ORCID iDs

He-Ji Huang https://orcid.org/0000-0002-1679-4736
Anthony B Murphy https://orcid.org/0000-0002-2820-2304
Hai-Xing Wang https://orcid.org/0000-0001-7426-0946

References

[1] Murphy A B and Uhrlandt D 2018 Foundations of high-pressure thermal plasmas *Plasma Sources Sci. Technol.* **27** 063001
[2] Murphy A B 2015 A perspective on arc welding research: the importance of the arc, unresolved questions and future directions *Plasma Chem. Plasma Process.* **35** 471–89

[3] Wang H X, Sun S R and Sun W P 2015 Status and prospects on nonequilibrium modeling of high velocity plasma flow in an arcjet thruster *Plasma Chem. Plasma Process.* **35** 534–64
[4] Wang H X, He Q S, Murphy A B, Zhu T and Wei F-Z 2017 Numerical simulation of nonequilibrium species diffusion in a low-power nitrogen–hydrogen arcjet thruster *Plasma Chem. Plasma Process.* **37** 877–95
[5] Pfender E 1976 Heat transfer from thermal plasmas to neighbouring walls or electrodes *Pure Appl. Chem.* **48** 199–213
[6] Pfender E and Heberlein J V R 2007 Heat transfer processes and modeling of arc discharges *Adv. Heat Transfer* **40** 345–450
[7] Nestor O H 1962 Heat intensity and current density distributions at the anode of high current, inert gas arcs *J. Appl. Phys.* **33** 1638–48
[8] Heberlein J V R, Mentel J and Pfender E 2010 The anode region of electric arcs: a survey *J. Phys. D: Appl. Phys.* **43** 023001
[9] Sun S R, Wang H X and Zhu T 2020 Numerical analysis of chemical reaction processes in different anode attachments of a high-intensity argon arc *Contrib. Plasma Phys.* **60** 201900094
[10] Sun S R, Wang H X, Zhu T and Murphy A B 2020 Chemical non-equilibrium simulation of anode attachment of an argon transferred arc *Plasma Chem. Plasma Process.* **40** 261–82
[11] Zhu T, Wang H X, Geng J Y, GENG J and Shen Y 2019 Numerical simulation of constricted and diffusive arc-anode attachments in wall-stabilized transferred argon arcs *Plasma Sci. Technol.* **21** 57–66
[12] Xia W D, Li L, Zhao Y, Ma Q, Du B, Chen Q and Cheng L 2006 Dynamics of large-scale magnetically rotating arc plasmas *Appl. Phys. Lett.* **88** 211501
[13] Wang C, Cui H, Zhang Z, Xia W and Xia W 2017 Observation of arc modes in a magnetically rotating arc plasma generator *Contrib. Plasma Phys.* **57** 395–403
[14] Wang C, Sun Q, Zhang Z, Zhang Z, Xia W and Xia W 2019 Experimental observations of constricted and diffuse anode attachment in a magnetically rotating arc at atmospheric pressure *Plasma Chem. Plasma Process.* **39** 407–21
[15] Schein J, Richter M, Landes K D, Forster G, Zierhut J and Dzulko M 2008 Tomographic investigation of plasma jets produced by multielectrode plasma torches *J. Therm. Spray Technol.* **17** 338–43
[16] Schein J, Zierhut J, Dzulko M, Forster G and Landes K D 2007 Improved plasma spray torch stability through multi-electrode design *Contrib. Plasma Phys.* **47** 498–504
[17] Huang H J, Pan W X and Wu C K 2018 Aerodynamic dispersion of anode arc attachment through a converging–diverging nozzle *IEEE Trans. Plasma Sci.* **47** 847–52
[18] Pan W X, Chen L W, Meng X, Zhang Y and Wu C 2016 Sufficiently diffused attachment of nitrogen arc by gasdynamic action *Theor. Appl. Mech. Lett.* **6** 293–6
[19] Wang C, Sun Q, Sun L, Lu Z, Xia W and Xia W 2019 Spot and diffuse mode of cathode attachments in a magnetically rotating arc plasma generator at atmospheric pressure *J. Appl. Phys.* **125** 033301
[20] Wang C, Sun Q, Zhang Z and Xia W 2020 Experimental observation and numerical analysis of the arc plasma axial motion in a magnetically rotating arc plasma generator *Plasma Phys. Rep.* **46** 617–26
[21] Sun J H, Sun S R, Wang H X, Niu C and ZHU T 2020 Comparative analysis of the arc characteristics inside the converging-diverging and cylindrical plasma torches *Plasma Sci. Technol.* **22** 034012
[22] Pan W X, Meng X, Li T, Xi C and Chengkang W 2007 Comparative observation of Ar, Ar–H_2 and Ar–N_2 dc arc plasma jets and their arc root behaviour at reduced pressure *Plasma Sci. Technol.* **9** 152–7
[23] Pan W X, Zhang W and Wu C K 2001 Generation of long laminar plasma jets at atmospheric pressure and effects of flow turbulence *Plasma Chem. Plasma Process.* **21** 23–35
[24] Shao K, Hu Y H, Meng X, Huang H-J, Sun S-R and Wang H-X 2021 Experimental study on the restrike mode of a dc arc anode attachment *Plasma Chem. Plasma Process.* **41** 1517–34
[25] Hu Y H *et al* 2021 A novel anode structure for diffuse arc anode attachment *J. Appl. Phys.* **54** 36LT01
[26] Guo H, Li P, Li H P, Ge N and Bao C-Y 2016 *In situ* measurement of the two-dimensional temperature field of a dual-jet direct-current arc plasma *Rev. Sci. Instrum.* **87** 033502
[27] Ge N, Wu G Q, Li H P, Wang Z and Bao C Y 2011 Evaluation of the two-dimensional temperature field and instability of a dual-jet dc arc plasma based on the image chain coding technique *IEEE Trans. Plasma Sci.* **39** 2884–5
[28] Wang Z, Wu G Q, Ge N, Li H-P and Bao C-Y 2010 Volt-ampere and thermal features of a direct-current dual-jet plasma generator with a cold gas injection *IEEE Trans. Plasma Sci.* **38** 2906–13